Title

Varying diffusion time to discriminate between simulated skeletal muscle injury models using stimulated echo diffusion tensor imaging

Journal

Magnetic Resonance in Medicine, 85(5)

ISSN

0740-3194

Authors

Berry, David B
Englund, Erin K
Galinsky, Vitaly
et al.

Publication Date

2021-05-01

DOI

10.1002/mrm.28598

Peer reviewed

HHS Public Access

Author manuscript

Magn Reson Med. Author manuscript; available in PMC 2021 June 15.

Published in final edited form as:

Magn Reson Med. 2021 May ; 85(5): 2524–2536. doi:10.1002/mrm.28598.

Varying diffusion time to discriminate between simulated skeletal muscle injury models using stimulated echo diffusion tensor imaging

David B. Berry[1], **Erin K. Englund**[2], **Vitaly Galinsky**[3,4], **Lawrence R. Frank**[4,5], **Samuel R. Ward**[2,6,7]

[1]Department of Nanoengineering, University of California San Diego, San Diego, California, USA

[2]Department of Orthopaedic Surgery, University of California San Diego, San Diego, California, USA

[3]Department of Electrical and Computer Engineering, University of California San Diego, San Diego, California, USA

[4]Center for Scientific Computation in Imaging, University of California San Diego, San Diego, California, USA

[5]Center for Functional MRI, University of California San Diego, San Diego, California, USA

[6]Department of Radiology, University of California San Diego, San Diego, California, USA

[7]Department of Bioengineering, University of California San Diego, San Diego, California, USA

Abstract

Purpose: Evaluate the relationship between muscle microstructure, diffusion time (Δ), and the diffusion tensor (DT) to identify the optimal Δ where changes in muscle fiber size may be detected.

Methods: The DT was simulated in models with histology informed geometry over a range of Δ with a stimulated echo DT imaging (DTI) sequence using the numerical simulation application DifSim. The difference in the DT at each Δ between healthy and injured skeletal muscle models was calculated, to identify the optimal Δ at which changes in muscle fiber size may be detected. The random permeable barrier model (RPBM) was used to estimate muscle microstructure from the simulated DT measurements, which were compared to the ground truth.

Results: Across all models, fractional anisotropy provided greater contrast between injured and control models than diffusivity measurements. Compared to control models, in atrophic injury models, the greatest difference in the DT was found between 90 ms and 250 ms. In models with

Correspondence: Samuel R. Ward, Departments of Orthopaedic Surgery, University of California San Diego, 9500 Gilman Drive (0863), La Jolla, CA 92093, USA. s1ward@health.ucsd.edu.

DATA AVAILABILITY STATEMENT

If you would like to request a copy of DifSim for testing and development, please visit: http://csci.ucsd.edu/software/difsim.html . The muscle model files are available at https://github.com/dbberry/muscle_models/.

SUPPORTING INFORMATION

Additional Supporting Information may be found online in the Supporting Information section.

acute edema, the contrast between injured and control muscle increased with increasing diffusion time, although these models had smaller mean fiber areas. RPBM systematically underestimated fiber size but accurately estimated surface area-to-volume ratio of simulated models.

Conclusion: These findings may better inform pulse sequence parameter selection when performing DTI experiments *in vivo*. If only a single diffusion experiment can be performed, the selected Δ should be ~170 ms to maximize the ability to discriminate between different injury models. Ideally several diffusion times between 90 ms and 500 ms should be sampled in order to maximize diffusion contrast, particularly when the disease process is unknown.

Keywords

diffusion tensor imaging; muscle fiber size; random permeable barrier model; skeletal muscle; stimulated echo; time-dependent diffusion

1 | INTRODUCTION

Skeletal muscle is a highly plastic tissue, able to alter its structural and functional properties based on environmental factors, such as exercise, disuse, injury, and pathology.[1,2] These factors often affect muscle fiber size, a key feature of muscle microstructure directly related to muscle fiber isometric force generating capacity.[1,3–5] Currently, the gold standard for assessing muscle fiber size is histology, which is highly invasive, destructive to the muscle, semi-quantitative, and only provides information about a fraction of the entire muscle volume. This has driven interest in developing quantitative, noninvasive techniques to study muscle microstructural changes resulting from injury for the clinical assessment of muscle pathology.

Diffusion tensor imaging (DTI) is an MRI technique used to assess restricted diffusion in skeletal muscle, which is thought to track microstructural and, thereby, functional changes. A key parameter in the DTI acquisition (or *pulse sequence*) is diffusion time (Δ); the time between two diffusion sensitizing gradient pulses. Previously, it has been demonstrated that prolonging Δ results in increased restricted diffusion transverse to the longitudinal axis of a muscle fiber (eg, radial diffusivity), with no change in diffusion parallel to the longitudinal axis of a fiber.[6–9] This suggests that radial diffusivity is likely restricted by the sarcolemma (cell membrane) of the muscle fiber, indicating that a relationship exists between radial diffusion, Δ, and fiber size. However, the amount of restricted diffusion relative to Δ for muscle with a given fiber size is unknown. Furthermore, the majority of studies that utilize DTI only acquire data at a single Δ due to scan time and signal-to-noise ratio (SNR) limitations.[10] Currently, there is no consensus on the optimal Δ that maximizes sensitivity to changes in muscle microstructure related to disease or injury, nor a consensus on how to interpret data acquired at different diffusion times.

Acquisition of diffusion-weighted data at multiple Δ, when scan time permits, may provide a more complete view of the relationship between muscle microstructure and the DT. As Δ increases, water molecules are able to diffuse over greater distances, increasing the possibility of interaction with and restriction by the sarcolemma. The time dependence of transverse diffusion in muscle fibers has led to the development and implementation of the

random permeable barrier model (RPBM) in order to estimate muscle microstructural parameters from the DT.[11] RPBM uses the time-dependent restricted diffusion profile of muscle to derive outcome measurements related to the underlying muscle microstructure including surface-to-volume ratio (S/V) and fiber diameter (a).[8,11] Generally, the microstructural effects observed with RPBM reflect expected changes in the microstructure, such as increasing fiber size during postnatal growth,[9] post exercise fiber dilation in healthy patients but not in patients with chronic extracellular compartment syndrome,[7] and decreased fiber size after rotator cuff repair.[8] However, RPBM routinely appears to underestimate fiber size measurements compared to histology, which is often acknowledged as a limitation. Although not perfect, this is currently the only model that directly relates the time-dependent DT to muscle fiber size.

The relationship between muscle microstructure, the diffusion time Δ, and the measured diffusion signal as a function of diffusion direction in healthy and injured muscle is complex and requires a systematic analysis if DTI is to be a useful clinical tool. *In silico* modeling allows for the precise control over simulated fiber size, fiber geometry, and Δ in order to calculate the resulting DT. Several groups have used in silico simulation to study the effect of imaging parameters on the DT such as SNR, diffusion directions, diffusion time, and diffusion weighting, in order to inform guidelines for developing DTI protocols.[12–19] Other studies have investigated the influence and sensitivity of microstructural features of muscle such as fiber geometry, diffusivity, and permeability on the DT.[17–21] No studies have systematically evaluated the relationship between muscle microstructure, Δ, and the DT. Furthermore, most modeling studies do not experimentally validate their results with acquired data.

Previously, we have used the DTI simulator DifSim, to investigate the sensitivity of a spin-echo DTI pulse sequence to muscle microstructure in histology informed models of healthy and injured skeletal muscle at a single short Δ.[20] However, spin-echo DTI pulse sequences cannot be used to assess the DT at long Δ due to the short T2 of muscle (~50 ms at 3T,[22] ~25 ms at 7T[23,24]). Stimulated echo DTI pulse sequences are an attractive alternative to spin-echo DTI pulse sequences, as they are less sensitive to T2 relaxation, which allows for DT measurements at long Δ.[25–27] Therefore, the goal of this study was to use DifSim to simulate a stimulated echo DTI pulse sequence on histologically informed models of healthy and injured muscle across a range of relevant Δ. In order to identify the optimal Δ at which changes in muscle fiber size may be detected, the difference in the DT at each Δ between healthy and injured skeletal muscle models was calculated. Furthermore, to identify how acquiring the DT at multiple Δ may increase the ability to discern between injured and healthy muscle, the DT's of these models at short, medium, and long Δ were compared. Additionally, the RPBM was used to estimate S/V and fiber size from the simulated DT measurements at all Δ and compared to known S/V and fiber size of the simulated models. Finally, in order to experimentally validate simulated DT measurements, the time-dependent DT between *in silico* simulated and *in situ* experimentally acquired data were directly compared.

2 | METHODS

The approach used in this study is similar to the approach used in a previous investigation of the same models using a spin-echo DTI sequence at a single Δ.[20] The "Overview of DifSim," "Histology informed model generation," and "Simulation details" sections of the methods section that follows have been previously reported.[20,28] All studies involving animals were approved by the University of California, San Diego Institutional Animal Care and Use Committee.

2.1 | Overview of DifSim

DifSim embeds MCell, a Monte Carlo simulator for cellular microphysiology,[29–31] within a MRI simulator which tracks particle location, magnetization amplitude, and phase, in a user defined arbitrarily complex geometrical model.[32,33] DifSim is capable of supporting boundary interactions, particle interactions, and multiple molecular species with different diffusion coefficients. A detailed explanation of DifSim can be found in Balls et al 2009.[32] A brief summary of DifSim can be found in Supporting Information, which is available online.

2.2 | Simulation DTI pulse sequence parameters

Pulse sequence parameters used in these MRI simulations were based on those used on a 7T MRI scanner at our institution (Bruker, Billerica MA).[34] A series of stimulated echo pulse sequences were simulated, with echo time (TE) = 21 ms, 15 gradient directions, voxel size = $200 \times 200 \times 200\ \mu m^3$, b = 500 s/mm^2, δ = 2 ms, and Δ = 20 ms, 30 ms, 40 ms, 50 ms, 90 ms, 130 ms, 170 ms, 250 ms, 325 ms, 400 ms, 500 ms, and 750 ms.

2.3 | Histology informed model generation

In order to relate the diffusion tensor to physiologically accurate models of muscle, we created models with geometry from previous animal histology experiments. Masson's Trichrome stained histology of muscle fibers from control, cardiotoxin injected, botulinum toxin (botox) injected, surgically denervated and surgically tenotomized rat tibialis anterior muscles at 1, 3, 7, 14 and 30 d post injury were used in this study. Cardiotoxin is venom from the *naja mossambica* snake, and induces depolarization of the sarcolemma that results in a massive, rapid onset muscle degeneration and inflammation, with new muscle fiber formation beginning at 3 d, from which muscle can heal in approximately 30 d.[35] Botox is a bacterium-produced neurotoxin that prevents acetylcholine release in motor neurons and results in muscle atrophy.[36,37] Surgical denervation creates a physical nerve injury that prevents a muscle from contracting, resulting in chronic atrophy.[38] Surgical tenotomy severs the tendon attaching muscle to bone, resulting in acute fiber hypertrophy due to isovolumetric contraction of the muscle, followed by chronic atrophy.[39] Average fiber diameters and S/V were recorded for each model. A detailed description of the injury models can be found in Supporting Information.

Histology informed models were generated from manually traced histology images that were extruded in the z-direction and triangulated using Blender[40] (Figure 1). Each histologic image was $600 \times 600\ \mu m^2$, which allowed for nine unique diffusion experiments to be

simulated, each with 200 μm isotropic voxels. Extracellular water volume fractions (corresponding to the magnitude of edema) were approximated from histologic and MRI studies of these tissues and assigned to each model (Table 1). No model was made with geometry from a day 1 cardiotoxin model, as there are no clearly defined muscle fibers at this timepoint.

2.4 | Simplified model generation

The complex polygonal, geometry of a muscle fiber was reduced to simple, tessellated hexagons, in order to minimize the number of defining characteristics of the model.[20] Fiber size was varied by systematically changing the diameter of the hexagon structures. Edema was simulated by varying the volume fraction of water in the "extracellular" space.

2.5 | Simulation details

Each model was simulated 10 times with a different initial location of diffusion particles to measure variance in an individual model. No noise was added in order to measure the exact relationship between muscle microstructure and the DT under ideal conditions. Intra- and extra-cellular particles were assigned different diffusion coefficients and magnetic relaxation (T1, T2) rates based on literature values of these tissues at 7T; intracellular: T1/T2: 1,740/25 ms,[23,24,41] D: $1.8*10^{-3}$ mm^2/s[42–44]; extracellular: T1/T2: 2,500/95 ms,[23,41] D: $2.2*10^{-3}$ mm^2/s.[45,46] Particles were defined as impermeable to the sarcolemma. A minimum of 200,000 particles were simulated in order to accurately converge on an analytical solution based on the diffusion coefficients and b-value chosen for this experiment.[32] Myofilaments within a muscle fiber, or extracellular matrix proteins outside of muscle fibers were not physically defined in this model, although it is at least partially reflected in the assigned diffusion coefficients, taken from previous studies of diffusion of small molecules in these tissues. All simulations were run on a Linux cluster with an Intel Xeon E-2697 CPU (2.60 GHz), with one node with 56 cores. The amount of time to run each simulation varied between 2 min and 54 h, depending on the number of particles simulated and the simulated Δ.

2.6 | Experimental data collection

Bilateral hindlimbs were obtained from three uninjured New Zealand White rabbits following sacrifice.[47] Data were collected using a 7T Bruker small animal imaging system (Bruker, Billerica MA). DTI data were collected using a stimulated echo diffusion-prepared sequence with a multi-shot echo planar imaging (EPI) readout and: repetition time (TR)/TE = 4700 ms/21.74 ms, field of view (FOV) = 48 × 40 mm^2, acquisition matrix = 120 × 62 (5/8th partial Fourier), reconstruction matrix = 120 × 100, segments = 4, slice thickness = 1 mm, number of slices = 5, averages = 4, directions = 15, targeted effective b = 500 s/mm^2, δ = 2 ms, Δ = 20 ms, 50 ms, 90 ms, 150 ms, 400 ms, scan time = 100 min 15 s. Following imaging, the tibialis anterior and soleus muscles were dissected, pinned and snap frozen. Histologic sections were obtained and stained with wheat germ agglutinin to stain the basement membrane, from which mean fiber size was calculated.

2.7 | DTI data processing

The analysis of functional neuroimages (AFNI) command 3dDWtoDT was used to calculate the DT for each voxel.[48] For the experimentally collected data, the effective b-matrix (calculated by the MRI scanner) was used to solve the DT, as the b-value in each direction is scaled due to the addition of imaging gradients.[49] Diagonalization of the DT yields the eigenvalues (λ1, λ2, and λ3), which were used to calculate mean diffusivity (MD), radial diffusivity (RD), and fractional anisotropy (FA):

$$MD = \frac{\lambda_1 + \lambda_2 + \lambda_3}{3} \tag{1}$$

$$RD = \frac{\lambda_2 + \lambda_3}{2} \tag{2}$$

$$FA = \sqrt{\frac{3}{2}} \sqrt{\frac{(\lambda_1 - MD)^2 + (\lambda_2 - MD)^2 + (\lambda_3 - MD)^2}{\sqrt{\lambda_1^2 + \lambda_2^2 + \lambda_3^2}}} \tag{3}$$

MD is a measure of the average overall diffusion. RD is a measure of diffusion orthogonal to the main axis (transverse diffusion). FA is a normalized scalar measure of how anisotropic the diffusion profile is and varies from 0 (perfectly isotropic) to 1 (perfectly anisotropic). Generally, as the restricted diffusion profile increases (increased FA), there is less overall diffusion (decreased MD, RD) and vice versa. The RPBM model and its implementation have been extensively discussed in Novikov et al[11] and Fieremans et al.[8] Briefly, the input arguments to the model are RD(Δ) and $\overline{\lambda 1}_{\Delta > 100\ \mathrm{ms}}$. From this model the free diffusion coefficient (D_0), the characteristic time scale associated with a single membrane (**τ**), and the effective "volume fraction" (**ζ**) are fit using nonlinear least squares analysis. From these parameters, **S/V** and fiber size (a) are derived:

$$S/V = \frac{2\zeta}{\sqrt{D_0 * \tau}} \tag{4}$$

$$a = \frac{2\sqrt{D_0 * \tau}}{\zeta} = \frac{4}{S/V} \tag{5}$$

2.8 | Statistics

In order to determine the Δ that maximizes contrast or difference in the DT profile between control and injured skeletal muscle, the difference between control and injured DT was calculated at each Δ for each injury timepoint. Bland Altman analyses were performed to assess agreement between the RPBM predicted and histologically obtained muscle microstructure measurements. All statistics were done in Prism (7.0c, La Jolla, CA). All data are presented as mean ± SD.

3 | RESULTS

3.1 | Muscle model microstructure

Average fiber diameter of the models ranged between 28.5 μm to 64.5 μm (Figure 2A). Average S/V of the models was 0.121/μm to 0.258/μm (Figure 2B). The average muscle fiber diameter of the control muscle was 56.7 μm ± 5.3 μm with an S/V of 0.135/μm ± 0.008/μm. Overall, atrophy models (botox, denervation, tenotomy) tended to have smaller fiber size and larger S/V than the control model except for tenotomy at days 1 and 3 due to acute unloading of the muscle. Cardiotoxin models demonstrated recovery of fiber size and S/V by 14 d, with overall larger muscle fibers and smaller S/V than control muscle at 30 d.

3.2 | Relationships between the DT and diffusion time for muscle injury models

Prolonging the diffusion time led to increased FA and decreased diffusivity, regardless of fiber size (Figure 3; Supporting Information Figure S1). Generally as a function of fiber area, FA was found to decrease, and diffusivity was found to increase as a model's mean fiber size increased. Models with edema (cardiotoxin day 3, 7, botox day 1) had lower FA and higher MD and RD, especially at longer diffusion times ($\Delta > 400$ ms), even though the mean fiber size was smaller than for models without edema. Additionally in models with edema, a plateau in DT measurements was observed at diffusion times greater than 400 ms, resulting in a different overall diffusion profile compared to models without edema.

3.3 | Difference in DT measurements between injured and control muscle

Across all models, FA provided greater contrast between injury models and the control model than diffusivity measurements, with a larger contrast observed for RD than MD (Figure 4; Supporting Information Figure S2). Compared to healthy muscle, botox and denervation models had the greatest contrast in FA at diffusion times between 130 ms and 250 ms. Generally, the greatest contrast for FA was found at $\Delta = 170$ ms and the greatest contrast for diffusivity measurements was found at $\Delta = 130$ ms. The difference between atrophic injury and the control model was found to increase as the difference in mean fiber size increased. Large differences in the DT were not observed in tenotomy models or in day 14 or 30 cardiotoxin models, likely because the models had similar fiber sizes to the control model. The largest contrast between control and tenotomy models was observed at day 30, with a difference in FA of 0.09 at 250 ms, which coincides with the largest difference in mean fiber size between the two models (−12.6 μm).

When comparing models with edema (cardiotoxin day 3, 7, botox day 1) to control muscle, a local maxima or minima in the diffusion profile between control and injury models was not observed (Figure 4; Supporting Information Figure S2). For example at small Δ, the day 7 cardiotoxin model was found to have a larger FA and smaller MD than control model, which is suggestive of smaller overall fibers. However, at long Δ this is reversed, with cardiotoxin having a smaller FA and larger diffusivity than control muscle which suggests larger muscle fibers, even though the cardiotoxin model has slightly smaller muscle fibers (−4 μm) than control muscle. Interestingly at $\Delta = 250$ ms, no effective difference in FA between control and the day 7 cardiotoxin model would be observed, while at smaller or larger Δ, a difference in magnitude in FA of up to 0.1 would be observed. This highlights the

importance of understanding how selection of Δ affects the ability to resolve microstructure driven differences in the DT between normal and injured skeletal muscle.

3.4 | DT in simplified models of muscle microstructure at short, medium, and long Δ

As fiber size and edema were determined to be the main microstructural features of muscle driving differences in the DT, models with a simplified, tessellated hexagon geometry were used to elucidate these relationships at short (50 ms), medium (170 ms), and long (400 ms) Δ. A normal muscle fiber diameter is approximately between 40 μm and 60 μm. For fibers in this span, the greatest dynamic range in the DT measurements was found for Δ = 170 ms for FA, MD, and RD (Figure 5A–C). Interestingly, these findings also demonstrate that, if the normal fiber diameter that one is expected to measure is smaller (eg, mouse; 20 μm to 40 μm), a shorter Δ of 50 ms may actually increase the dynamic range of DT measurements, increasing sensitivity to detect changes in this range. Generally, the dynamic range of the DT in muscles with larger average fiber size (>60 μm) is similar across short, medium, and long diffusion times. For models simulating edema, as the extracellular volume fraction increased, the DT measurements made at short, medium, and long diffusion times were found to converge (Figure 5D–F). In comparison to models varying fiber size, edema was found to have less of an effect on the diffusion tensor overall at short, medium, and long diffusion times.

3.5 | RPBM model to predict muscle microstructure

Key output variables from the RPBM model included D_0, τ, and ζ, which were used to estimate S/V and fiber size of the histology informed muscle models. RPBM was found to systematically underestimate fiber size compared to the actual diameter of the muscle fibers in the model for each voxel for each simulated model, with a bias of 22.6 μm ± 7.1 μm (Figure 6A,B). However, RPBM was found to accurately predict actual S/V of the muscle fibers simulated in this study (Figure 6C,D). When actual fiber diameter was compared to the RPBM estimated S/V of each model, an inverse relationship between the two variables was observed (Figure 6E,F).

Given that Equation 9 from Novikov et al[11] is an approximate relationship derived from the geometry of a square lattice and not from actual muscle microstructure, a physiology based supplementary analysis was performed. Fiber diameter, area, and S/V was measured from 14,221 muscle fibers with geometry extracted from separate histology not used for the simulation models of control and a botox injury model at acute and chronic timepoints after injury. An inverse relationship was found between S/V and both fiber diameter $\left(=\frac{6.29}{S/V}\right)$ and area $\left(=\frac{99.1m}{S/V}\right)$, with inverse nonlinear regression explaining 89.5% and 87.0% of the variance in the models, respectively (Figure 7).

3.6 | Comparing simulated and experimentally acquired time-dependent diffusion data

The average fiber diameter of the skeletal muscle from the experimentally acquired DT data was 50.0 μm ± 10.0 μm. The average fiber diameter from the simulated DT data was 49.5 μm ± 2.4 μm. The apparent diffusion coefficient (ADC) in experimentally acquired data was 1.2×10^{-3} mm^2/s, which was lower than that used for simulation (1.8×10^{-3} mm^2/s).

Therefore, to account for the offset in diffusivity between measured and simulated experiments, MD and RD were normalized to their respective ADC. Experimental MD/ADC and RD/ADC decreased as a function of diffusion time, in agreement with the simulation data (Figure 8). In general, FA increased over the range of diffusion times and was in good agreement between both the simulation and experimental data.

4 | DISCUSSION AND CONCLUSIONS

DTI has the potential to be a useful clinical tool if it can successfully identify microstructural changes that are associated with injury, disease, or aging. As fiber size is a fundamental metric of muscle health, understanding the limits of DTI's sensitivity to fiber size is important if DTI is to be adopted as a functional alternative to invasive biopsy and histology. Furthermore, these findings can be used to select a Δ that will maximize the statistical SNR in the DT measurements (note: not signal to noise ratio of the images themselves) between normal and injured muscle, which in turn can be used to minimize sample sizes for between group comparisons.

In this study, we evaluated how Δ affects the resulting DT through simulation in physiologically relevant models of muscle injury. Driven by fiber size variation and simulated edema, differences in the diffusion profile were observed between muscle injury models with increasing Δ. In atrophic models without edema, maximum contrast between healthy and injured skeletal muscle was found between diffusion encoding times of 130 ms and 250 ms. In models with larger or similar average fiber size compared to control, small differences in the DT were found at all Δ, with no clear time where there was maximum contrast compared to control models. This suggests that DTI may not be as sensitive to detecting muscle hypertrophy compared to muscle atrophy, depending on the extent of relative change in fiber size. This is supported by our previous study and the models with simplified geometry in this study, which demonstrated increased sensitivity to atrophy and decreased sensitivity to hypertrophy in DTI-based measurements of muscle microstructure.[20] In models with simulated edema, a different characteristic diffusion profile was observed compared to non-edematous muscle; lower FA and increased diffusivity were observed at long Δ. Compared to the control muscle, these findings demonstrate that only measuring the DT at a single Δ in edematous muscles may result in improper characterization of the underlying muscle microstructure.

If only a single Δ can be measured, a Δ between 130 ms and 250 ms maximizes sensitivity to detecting muscle atrophy for physiologically relevant muscle fiber sizes (40 μm-60 μm). However, as mentioned previously, this approach is prone to mischaracterizing underlying microstructure if significant edema is present. Therefore, when scan time permits, we propose that the DT be measured at a minimum of three Δ—short ($\Delta < 90$ ms), medium (130 ms $< \Delta <$ 250 ms), and long ($\Delta >$ 400 ms)—from which a more complete understanding of how underlying microstructure influences the DT may be attained. For example, if a muscle is undergoing atrophy, at short Δ slightly elevated FA compared to control would be observed, with a larger elevation of FA observed at a medium Δ, and an FA between short Δ and medium Δ at long Δ. However, if a slightly elevated FA was observed at short Δ and a decreased FA compared to control was observed at long Δ, this may indicate edema is

present. The expected difference between injured and control muscle for FA and diffusivity measurements for atrophic, hypertrophic, and edematous muscle are summarized in Table 2.

A secondary goal of this study was to evaluate the ability of the RPBM model to predict muscle fiber size. While the RPBM model was found to systematically underestimate muscle fiber size, it accurately estimated the S/V ratio. When directly compared, RPBM predicted S/V ratio appeared to be inversely related to the actual fiber size. However, the dynamic range of S/V was greatest for fiber diameters less than 50 μm, indicating that S/V may be more sensitive to muscle atrophy than hypertrophy. While, S/V is traditionally not measured in histological assessments of muscle, diameter and area are common metrics of muscle health as they are related to whole muscle function.[1,3–5] To investigate the potential relationship between fiber diameter, area, and S/V over a physiologically relevant range of fiber sizes in healthy and injured muscle, a supplementary analysis was performed on 14,221 muscle fibers with histology informed geometry. Since S/V is a direct output measurement of the RPBM model, and fiber size is based on an approximation, a physiology informed conversion from S/V to fiber size was determined to be more appropriate than simply scaling in order to fit the RPBM model alone. This analysis determined that $a = \frac{6.29}{S/V}$ is a more appropriate relationship to convert RPBM measured S/V to estimated muscle fiber size than the previous conversion (Equation 5), which was based on the geometry of a square lattice.

This study used a stimulated echo DTI pulse sequence, as the Δ's probed in this study are not feasible using the spin-echo DTI pulse sequence used in our prior simulation study.[20] Spin-echo pulse sequences are sensitive to the short T2 relaxation of skeletal muscle as a result of the relatively long TEs that are required to apply diffusion weighting. This generally limits Δ to ~40 ms or less in most spin-echo DTI-based studies of muscle microstructure, with even shorter Δ at higher magnetic field strengths.[23,50] However, even at shorter diffusion times (Δ = 9 ms), we have demonstrated that fiber size accounts for 40% of the variance in the DT using spin-echo DTI, and up to 70% of the variance in the DT when a multi-echo spin-echo DTI pulse sequence is used to separate diffusion from the intracellular and extracellular compartments based on differences in compartmental T2 relaxation.[20] The results from the present study indicate that, when edema is present, there is less contrast between models with different fiber sizes and the diffusion signal arising from the increased extracellular water is dominating the overall diffusion signal, especially at long Δ. While spin-echo DTI may not have the same sensitivity to muscle fiber size as stimulated echo DTI in non-edematous muscle, in the presence of edema, multi-echo spin-echo DTI may provide enhanced sensitivity to muscle fiber size compared to stimulated echo DTI. Therefore, the decision to use a spin-echo or a stimulated echo DTI pulse sequence to monitor muscle fiber size may be informed by the potential inflammatory state of the muscle.

All of the simulations in this study were performed with no noise in order to investigate the precise relationship between microstructure and the DT. As stimulated echo DTI pulse sequences only refocus half of the magnetization, they have a lower SNR than spin-echo DTI pulse sequences at the same TE. Therefore, the DT calculated from stimulated echo DTI is more susceptible to noise. Under low SNR conditions, λ3 is typically underestimated, resulting in overestimation of FA.[12] This is likely to decrease the sensitivity

of FA and RD to detect fiber size differences between muscles. Prior studies have demonstrated that the minimum SNR required to get accurate DT measurements is 20.[12,51] Therefore, future studies will investigate the effect of noise on the ability to discern differences in the DT in models of known muscles size at the optimal Δ under low SNR (<20), minimum SNR,[20] and high SNR (>40) conditions.

An additional goal of this study was to validate the simulated findings by comparing DT measurements in simulated models with histology informed geometry and real muscle tissue under similar imaging parameters. Relative agreement between the trajectory of MD, RD, and FA were found between simulated and experimentally acquired data over the diffusion times evaluated. The reduced ADC in unnormalized experimental data was likely due to thermally driven differences in the diffusion of water, as the tissue was from sacrificed animals and scanned at room temperature. There is an expected 2%/°C change in ADC as a function of temperature.[52] While the sample temperature was not explicitly measured, if we assume body temperature = 37°C and room temperature = 21°C, this would result in a reduction of ADC by about 30%, which would result in and ADC = 1.26×10^{-3} mm^2/s, similar to what was experimentally measured (ADC = 1.2×10^{-3} mm^2/s). This phenomenon may explain that, when MD and RD were normalized by ADC, good agreement in the DT was found between simulated and experimentally acquired measurements at multiple Δ. This highlights the relationship between diffusion and temperature; if the overall diffusion is lower, the mean squared displacement of diffusing particles decreases, resulting in fewer potential interactions with the restrictive membrane. Future in situ MRI scans will be performed using a heating pad in order to standardize diffusion measurements at body temperature. Additionally, a future in silico study will investigate the relationship between the DT and muscle microstructure as a function of thermally controlled diffusion.

Fatty infiltration and fibrosis are common hallmarks of muscle degeneration often occurring in parallel with, or secondary to muscle atrophy. In particular, fat has consistently been demonstrated to confound DTI measurements in patients with neuromuscular degenerative disorders.[51,53] Generally, increased fat signal percentage has been shown to decrease overall diffusivity and increase fractional anisotropy.[53] To combat this, several groups implement fat suppression techniques in order to isolate the diffusion signal originating from muscle tissue.[53–55] In the context of this study, the histology informed models came from rat injury models, which traditionally demonstrate very low overall fatty infiltration and any fat signal is unlikely to significantly alter the overall effect of the diffusion signal. Future simulation studies will systematically evaluate the role of fatty infiltration on diffusion measurements from histology informed models of human neuromuscular degeneration. The effect of fibrosis on the diffusion signal is less clear. Previously, we have evaluated the effect of fibrosis using a simplified model; increasing the spacing between muscle fibers.[20] Of the four main muscle microstructural features evaluated (fibrosis, fiber size, permeability, edema), fibrosis was routinely found to have the least overall effect on the diffusion signal. Furthermore, collagenous tissues present in fibrosis generally have an extremely short T2 relaxation time, which is difficult to assess using traditional spin-echo and stimulated echo preparations. However, fibrosis is a complicated biological process that results in tissue properties that are not easily characterized and, thus, difficult in which to model the diffusion effects.

This study had a few limitations. The models in this study were of 2D structures that were extrapolated into 3D, because it is difficult to histologically assess 3D geometry of multiple muscle fibers. However, it should be noted that this is also an assumption in histology, and that muscle fiber geometry is relatively uniform longitudinally; therefore, slight variations in longitudinal microstructure are unlikely to significantly affect the DT. Additionally, small extracellular and intracellular structures (ie, collagen, myofilaments) were not directly modeled, as they could not be clearly identified from histology. The presence of these structures was partially accounted for by the assigned diffusion coefficients for particles in these regions as they were derived from studies measuring the diffusivity of small macromolecules around these structures. Another limitation of this study was that the simulated model that was compared to the experimentally acquired data was generated from rat histology with nearly identical fiber size (acquired 50.0 μm vs simulated 49.5 μm), not from histology from the rabbits themselves. This was chosen because fiber size is considered the primary barrier to diffusion, and there is no evidence that the diffusion coefficient of water in muscle varies between species. Future comparisons between simulated and acquired data will use histology from the acquired data to generate in silico models. Finally, at prolonged Δ in experimentally collected data, slice selection gradients substantially contribute to the effective b-value. In order to account for this, the nominal b-value was adjusted such that the effective b-value would remain ~500 s/mm^2 (Supporting Information Figure S3). Furthermore, to account for directional variations in the effective b-value in experimentally collected data, the b-matrix was used to solve for the DT.

Using in silico modeling to carefully relate microstructural features of muscle to the DT allows for precise control over the entire diffusion experiment. The findings of this study provide a framework for identifying what single Δ, or combination of Δ may provide the most accurate interpretation of the relationship between DTI measurements and muscle microstructure. Furthermore, this study also helped to independently validate RPBM as potential tool to translate DTI data to the underlying muscle microstructure, when scan time allows for multiple Δ to be sampled. RPBM was found to accurately predict S/V of muscle fibers and is inversely correlated with fiber size. The sub-analysis in this study determined a better conversion between S/V and fiber size measurements, which may increase the accuracy of RPBM for predicting muscle fiber size. Taken together, these findings explore how to maximize sensitivity of DTI to muscle microstructure so that this technique can be used clinically with the long-term goal of noninvasively identifying disease, monitoring disease progression, evaluating treatments, and reducing the need for muscle biopsies.

Supplementary Material

Refer to Web version on PubMed Central for supplementary material.

Funding information

National Institute of Health, Grant/Award Number: R01AR070830

REFERENCES

1. Lieber RL. Skeletal Muscle Structure, Function, and Plasticity: The Physiological Basis of Rehabilitation. Philadelphia: Lippincott Williams & Wilkins; 2010.
2. Frontera WR, Ochala J. Skeletal muscle: A brief review of structure and function. Calcif Tissue Int. 2015;45:183–195.
3. Krivickas LS, Dorer DJ, Ochala J, Frontera WR. Relationship between force and size in human single muscle fibres. Exp Physiol. 2011;96:539–547. [PubMed: 21317219]
4. Ward SR, Minamoto VB, Suzuki KP, Hulst JB, Bremner SN, Lieber RL. Recovery of rat muscle size but not function more than 1 year after a single botulinum toxin injection. Muscle Nerve. 2018;57:435–441. [PubMed: 28556093]
5. Fitts RH, McDonald KS, Schluter JM. The determinants of skeletal muscle force and power: Their adaptability with changes in activity pattern. J Biomech. 1991;24:111–122. [PubMed: 1791172]
6. Kim S, Chi-Fishman G, Barnett AS, Pierpaoli C. Dependence on diffusion time of apparent diffusion tensor of ex vivo calf tongue and heart. Magn Reson Med. 2005;54:1387–1396. [PubMed: 16265644]
7. Sigmund EE, Novikov DS, Sui D, et al. Time-dependent diffusion in skeletal muscle with the random permeable barrier model (RPBM): application to normal controls and chronic exertional compartment syndrome patients. NMR Biomed. 2014;27:519–528. [PubMed: 24610770]
8. Fieremans E, Lemberskiy G, Veraart J, Sigmund EE, Gyftopoulos S, Novikov DS. In vivo measurement of membrane permeability and myofiber size in human muscle using time-dependent diffusion tensor imaging and the random permeable barrier model. NMR Biomed. 2017;30:e3612.
9. Winters KV, Reynaud O, Novikov DS, Fieremans E, Kim SG. Quantifying myofiber integrity using diffusion MRI and random permeable barrier modeling in skeletal muscle growth and Duchenne muscular dystrophy model in mice. Magn Reson Med. 2018;80:2094–2108. [PubMed: 29577406]
10. Oudeman J, Nederveen AJ, Strijkers GJ, Maas M, Luijten PR, Froeling M. Techniques and applications of skeletal muscle diffusion tensor imaging: A review. J Magn Reson Imaging. 2016;43:773–788. [PubMed: 26221741]
11. Novikov DS, Fieremans E, Jensen JH, Helpern JA. Random walks with barriers. Nat Phys. 2011;7:508–514. [PubMed: 21686083]
12. Damon BM. Effects of image noise in muscle diffusion tensor (DT)-MRI assessed using numerical simulations. Magn Reson Med. 2008;60:934–944. [PubMed: 18816814]
13. Damon BM. Effect of b-value and TE on the estimation of intramyocellular diffusion properties in the presence of edema. In: Proceedings 17th Scientific Meeting, International Society for Magnetic Resonance in Medicine. Vol. 17; 2009. p 1435.
14. Pierpaoli C, Basser PJ. Toward a quantitative assessment of diffusion anisotropy. Magn Reson Med. 1996;36:893–906. [PubMed: 8946355]
15. Anderson AW. Theoretical analysis of the effects of noise on diffusion tensor imaging. Magn Reson Med. 2001;46:1174–1188. [PubMed: 11746585]
16. Farrell JAD, Landman BA, Jones CK, et al. Effects of signal-to-noise ratio on the accuracy and reproducibility of diffusion tensor imaging-derived fractional anisotropy, mean diffusivity, and principal eigenvector measurements at 1.5T. J Magn Reson Imaging. 2007;26:756–767. [PubMed: 17729339]
17. Hall MG, Clark CA. Diffusion in hierarchical systems: A simulation study in models of healthy and diseased muscle tissue. Magn Reson Med. 2017;78:1187–1198. [PubMed: 27667781]
18. Naughton NM, Georgiadis JG. Global sensitivity analysis of skeletal muscle dMRI metrics: Effects of microstructural and pulse parameters. Magn Reson Med. 2020;83:1458–1470. [PubMed: 31612545]
19. Froeling M, Nederveen AJ, Nicolay K, Strijkers GJ. DTI of human skeletal muscle: The effects of diffusion encoding parameters, signal-to-noise ratio and T2 on tensor indices and fiber tracts. NMR Biomed. 2013;26:1339–1352. [PubMed: 23670990]
20. Berry DB, Regner B, Galinsky V, Ward SR, Frank LR. Relationships between tissue microstructure and the diffusion tensor in simulated skeletal muscle. Magn Reson Med. 2018;80:317–329. [PubMed: 29090480]

21. Karampinos DC, King KF, Sutton BP, Georgiadis JG. Myofiber ellipticity as an explanation for transverse asymmetry of skeletal muscle diffusion MRI in vivo signal. Ann Biomed Eng. 2009;37:2532–2546. [PubMed: 19763830]
22. Stanisz GJ, Odrobina EE, Pun J, et al. T1, T2 relaxation and magnetization transfer in tissue at 3T. Magn Reson Med. 2005;54:507–512. [PubMed: 16086319]
23. Fan RH, Does MD. Compartmental relaxation and diffusion tensor imaging measurements *in vivo* in λ-carrageenan-induced edema in rat skeletal muscle. NMR Biomed. 2008;21:566–573. [PubMed: 18041804]
24. Crémillieux Y, Ding S, Dunn JF. High-resolutionin vivo measurements of transverse relaxation times in rats at 7 Tesla. Magn Reson Med. 1998;39:285–290. [PubMed: 9469712]
25. Tanner JE, Annert JET. Restricted self-diffusion of protons in colloidal systems by the pulsed-gradient. Restricted Diffus. Flow J Chem Phys. 1970;52:3597.
26. Frahm J, Merboldt K, Hänicke W, Haase A. Stimulated echo imaging. J Magn Reson. 1985;64:81–93.
27. Von Deuster C, Stoeck CT, Genet M, Atkinson D, Kozerke S. Spin echo versus stimulated echo diffusion tensor imaging of the in vivo human heart. Magn Reson Med. 2016;76:862–872 [PubMed: 26445426]
28. Berry DB, Englund EK, Frank LR, Ward SR. Simulated effect of diffusion time and skeletal muscle fiber size on the diffusion tensor. In: International Society for Magnetic Resonance in Medicine. Montreal; 2019.
29. Stiles JR, Bartol TM. Monte Carlo methods for simulating realistic synaptic microphysiology using MCell. In: Computational Neuroscience: Realistic Modeling for Experimentalists. Boca Raton, FL: Boca Raton: CRC Press; De Schutter E, ; 2001:87–127.
30. Stiles JR, Van Helden D, Bartol TM, Salpeter EE, Salpeter MM. Miniature endplate current rise times <100 μs from improved dual recordings can be modeled with passive acetylcholine diffusion from a synaptic vesicle. Proc Natl Acad Sci USA. 1996;93:5747–5752. [PubMed: 8650164]
31. Kerr RA, Bartol TM, Kaminsky B, et al. Fast Monte Carlo simulation methods for biological reaction-diffusion systems in solution and on surfaces. SIAM J Sci Comput. 2008;30:3126–3149. [PubMed: 20151023]
32. Balls GT, Frank LR. A simulation environment for diffusion weighted MR experiments in complex media. Magn Reson Med. 2009;62:771–778. [PubMed: 19488991]
33. Baxter GT, Frank LR. A computational model for diffusion weighted imaging of myelinated white matter. Neuroimage. 2013;75:204–212. [PubMed: 23507381]
34. Berry DB, You S, Warner J, Frank LR, Chen S, Ward SR. A 3D tissue-printing approach for validation of diffusion tensor imaging in skeletal muscle. Tissue Eng Part A. 2017;23:980–988. [PubMed: 28338417]
35. d'ALBIS A, Couteaux R, Janmot C, Roulet A, Mira J-C. Regeneration after cardiotoxin injury of innervated and denervated slow and fast muscles of mammals. Myosin isoform analysis. Eur J Biochem. 1988;174:103–110. [PubMed: 3371354]
36. Dolly O Synaptic transmission: Inhibition of neurotransmitter release by botulinum toxins. Headache J Head Face Pain. 2003;43:16–24.
37. Brin MF. Botulinum toxin: Chemistry, pharmacology, toxicity, and immunology. Muscle Nerve Suppl. 1997;6:S146–S168. [PubMed: 9826987]
38. Kobayashi J, Mackinnon SE, Watanabe O, et al. The effect of duration of muscle denervation on functional recovery in the rat model. Muscle Nerve. 1997;20:858–866. [PubMed: 9179158]
39. Józsa L, Kannus P, Thöring J, Reffy A, Järvinen M, Kvist M. The effect of tenotomy and immobilisation on intramuscular connective tissue. A morphometric and microscopic study in rat calf muscles. J. Bone Joint Surg. Br 1990;72:293–297. [PubMed: 2312572]
40. Kent BR. 3D Scientific Visualization with Blender. San Rafael: Morgan & Claypool Publishers; 2015.
41. Diakova G, Korb J-P, Bryant RG. The magnetic field dependence of water T1 in tissues. Magn Reson Med. 2012;68:272–277. [PubMed: 22144333]

42. Papadopoulos S, Jürgens KD, Gros G. Protein diffusion in living skeletal muscle fibers: Dependence on protein size, fiber type, and contraction. Biophys J. 2000;79:2084–2094. [PubMed: 11023912]
43. Moll W The diffusion coefficient of myoglobin in muscle homogenate. Pflugers Arch Gesamte Physiol Menschen Tiere. 1968;299:247–251.
44. Gefen A, Cornelissen LH, Gawlitta D, Bader DL, Oomens CWJ. The free diffusion of macromolecules in tissue-engineered skeletal muscle subjected to large compression strains. J. Biomech 2008;41:845–853. [PubMed: 18068175]
45. Gilbert DL, Okano T, Miyata T, Kim SW. Macromolecular diffusion through collagen membranes. Int J Pharm. 1988;47:79–88.
46. Ramanujan S, Pluen A, McKee TD, Brown EB, Boucher Y, Jain RK. Diffusion and convection in collagen gels: Implications for transport in the tumor interstitium. Biophys J. 2002;83:1650–1660. [PubMed: 12202388]
47. Englund EK, Berry DB, Galinsky V, Frank LR, Ward SR. Comparison of simulated and experimental stimulated echo diffusion at varying diffusion times in skeletal muscle. In: In Proceedings of the ISMRM & SMRT Virtual Conference & Exhibition, 2020. Sydney; 2020.
48. Cox RW. AFNI: Software for analysis and visualization of functional magnetic resonance neuroimages. Comput Biomed Res. 1996;29:162–173. [PubMed: 8812068]
49. Mattiello J, Basser PJ, Le Bihan D. The b matrix in diffusion tensor echo-planar imaging. Magn Reson Med. 1997;37:292–300. [PubMed: 9001155]
50. Heemskerk AM, Drost MR, van Bochove GS, van Oosterhout MFM, Nicolay K, Strijkers GJ. DTI-based assessment of ischemia-reperfusion in mouse skeletal muscle. Magn Reson Med. 2006;56:272–281. [PubMed: 16826605]
51. Hooijmans MT, Damon BM, Froeling M, et al. Evaluation of skeletal muscle DTI in patients with duchenne muscular dystrophy. NMR Biomed. 2015;28:1589–1597. [PubMed: 26449628]
52. Morvan D, Leroy-Willig A, Jehenson P, Cuenod CA, Syrota A. Temperature changes induced in human muscle by radio-frequency H-1 decoupling: Measurement with an MR imaging diffusion technique. Work in progress. Radiology. 1992;185:871–874. [PubMed: 1438778]
53. Williams SE, Heemskerk AM, Welch EB, Li K, Damon BM, Park JH. Quantitative effects of inclusion of fat on muscle diffusion tensor MRI measurements. J Magn Reson Imaging. 2013;38:1292–1297. [PubMed: 23418124]
54. Burakiewicz J, Hooijmans MT, Webb AG, Verschuuren JJGM, Niks EH, Kan HE. Improved olefinic fat suppression in skeletal muscle DTI using a magnitude-based dixon method. Magn Reson Med. 2018;79:152–159. [PubMed: 28261865]
55. Hooijmans MT, Froeling M, Koeks Z, et al. Multi-parametric MR in Becker muscular dystrophy patients. NMR Biomed. 2020;33:e4385. [PubMed: 32754921]

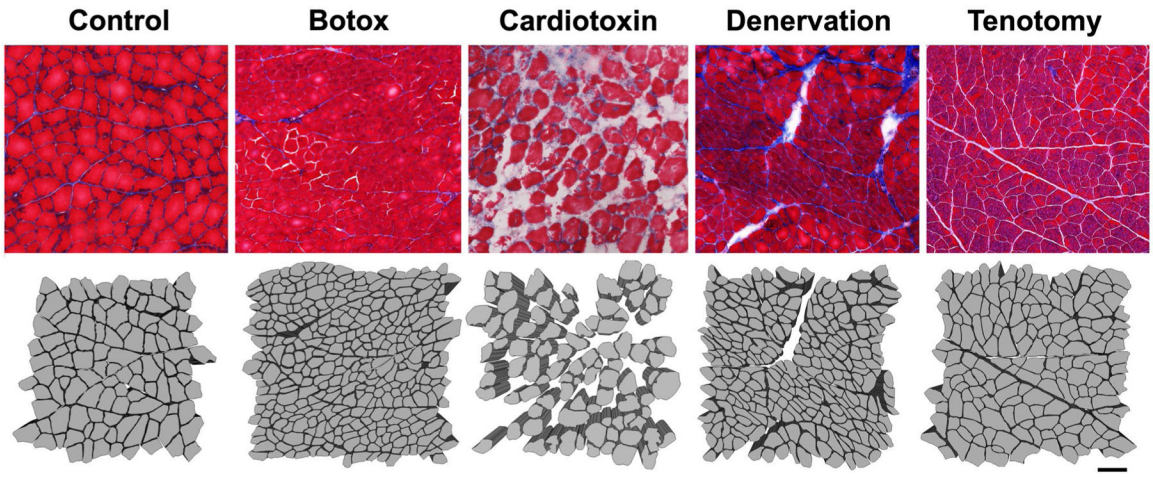

FIGURE 1.

Schematic depicting histology informed models of skeletal muscle. Botox, denervation, and tenotomy models are from animals 30 d post injury. Cardiotoxin models are from animals 3 d post injury. Scale bar indicates 100 μm

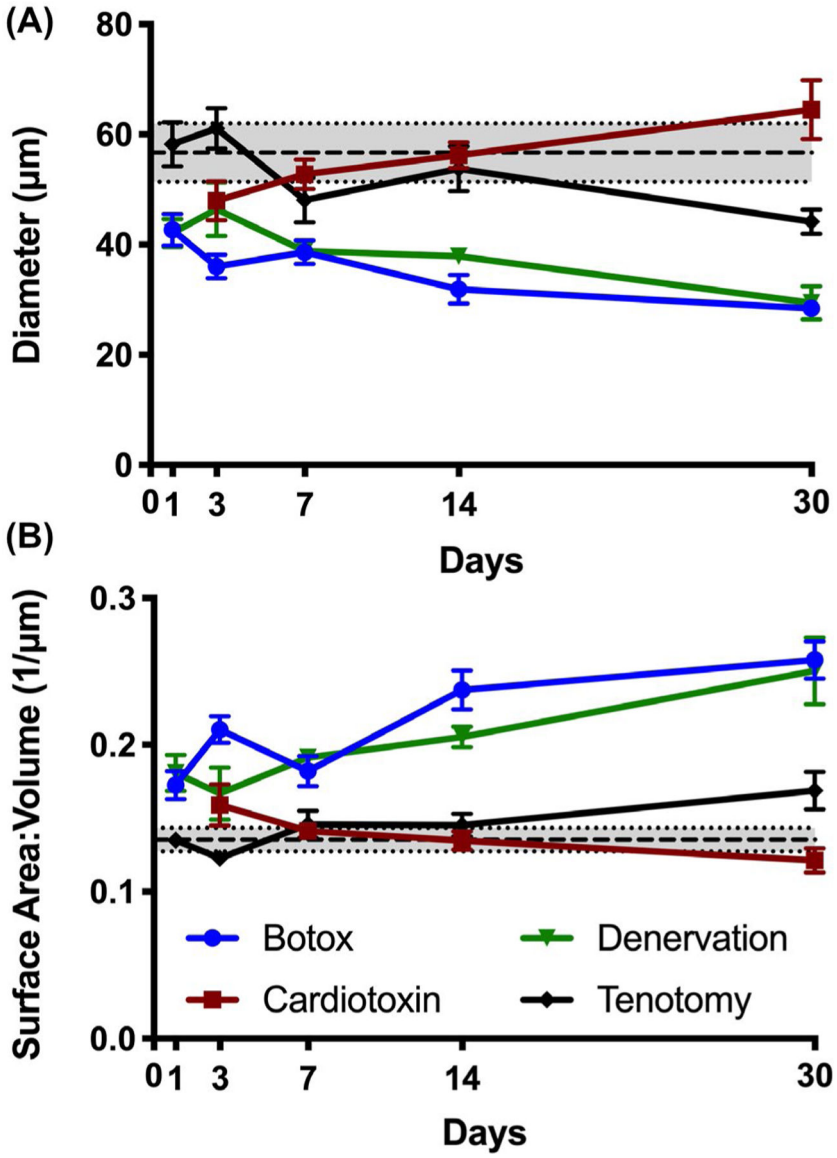

FIGURE 2.

Average fiber diameter (A) and surface area to volume ratio (B) for each model at all post-injury time points. Gray area represents mean ± SD of control, uninjured muscle

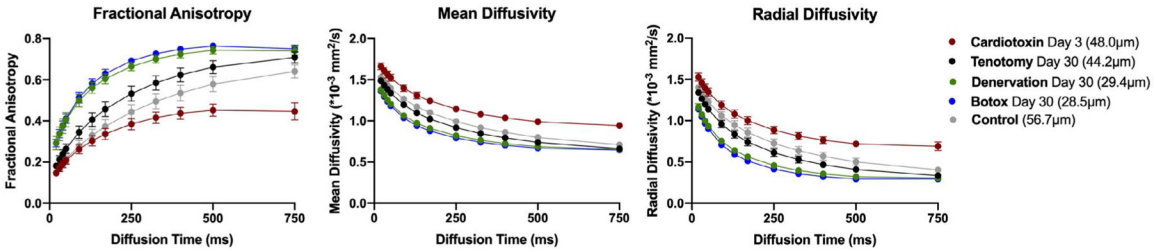

FIGURE 3.

Example fractional anisotropy (left), mean diffusivity (middle), and radial diffusivity (right) from each injury model at each diffusion time. Mean fiber size of each model at each time point is reported in the figure legend. Full results can be found in Supporting Information Figure S1

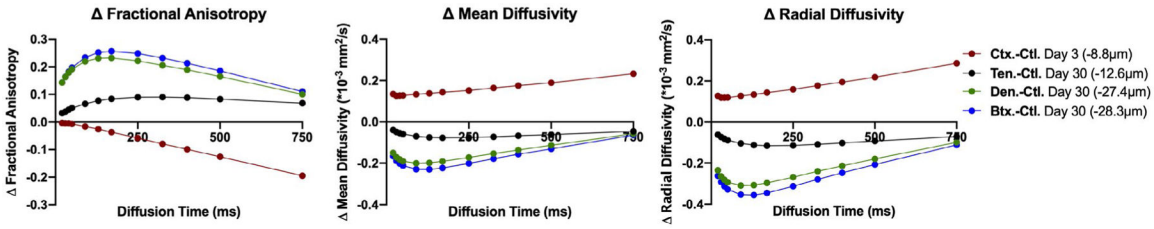

FIGURE 4.

Example difference in fractional anisotropy (left), mean diffusivity (middle), and radial diffusivity (right) between the control and injured model at each diffusion time. A positive difference indicates that the injury model has a larger diffusion measurement at that time point. The difference in mean fiber size between the control and injury models at each time point is reported in the figure legend. Full results can be found in Supporting Information Figure S2

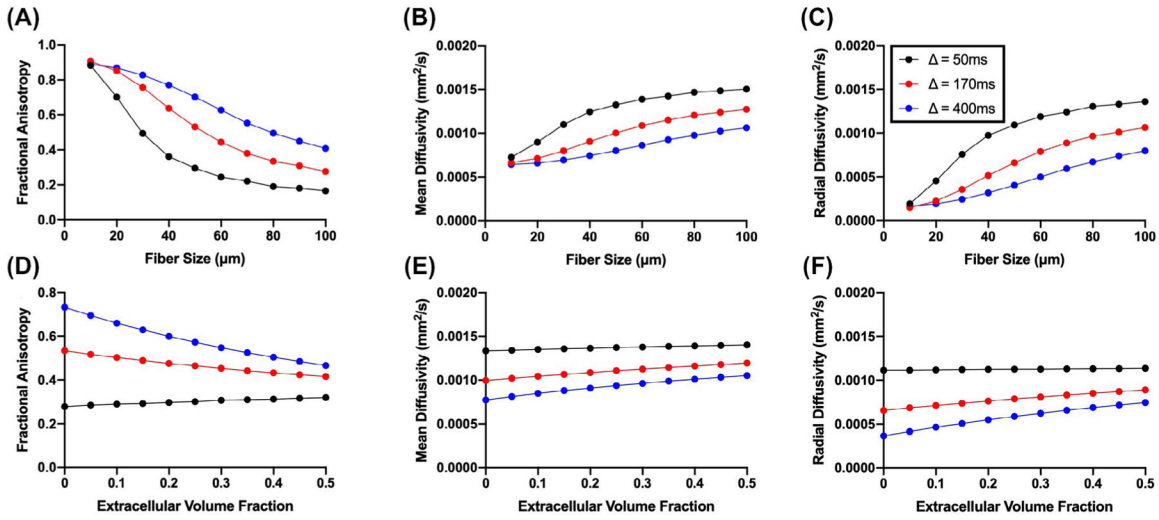

FIGURE 5.

Diffusion tensor measurements for models with simplified microstructure. Models with varying fiber size (A-C) and extracellular water volume fraction (D-F), related to edema, were evaluated at short (black; 50 ms), medium (red; 170 ms), and long (blue; 400 ms) diffusion times (Δ)

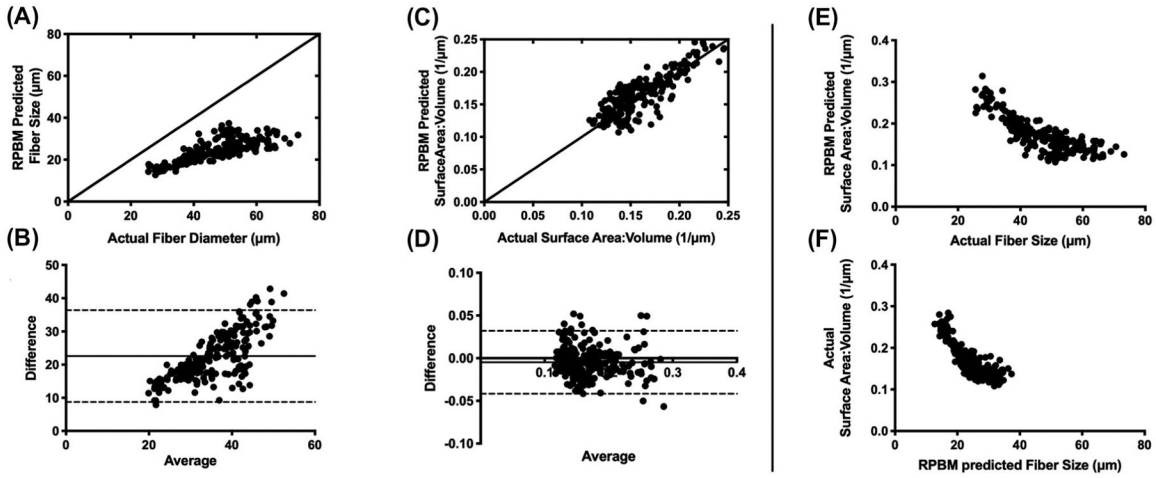

FIGURE 6.

RPBM predicted versus actual fiber size (A) and surface area to volume ratio (C). The identity line is included in A and C. Bland Altman analysis reveals RPBM systematically underestimates fibers size (B) but accurately estimates surface area to volume ratio (D). The magnitude of fiber size underestimation increases with increasing actual fiber size. E) RPBM predicted surface area to volume ratio versus actual fiber size. F) Actual surface area to volume ratio versus RPBM predicted fiber size

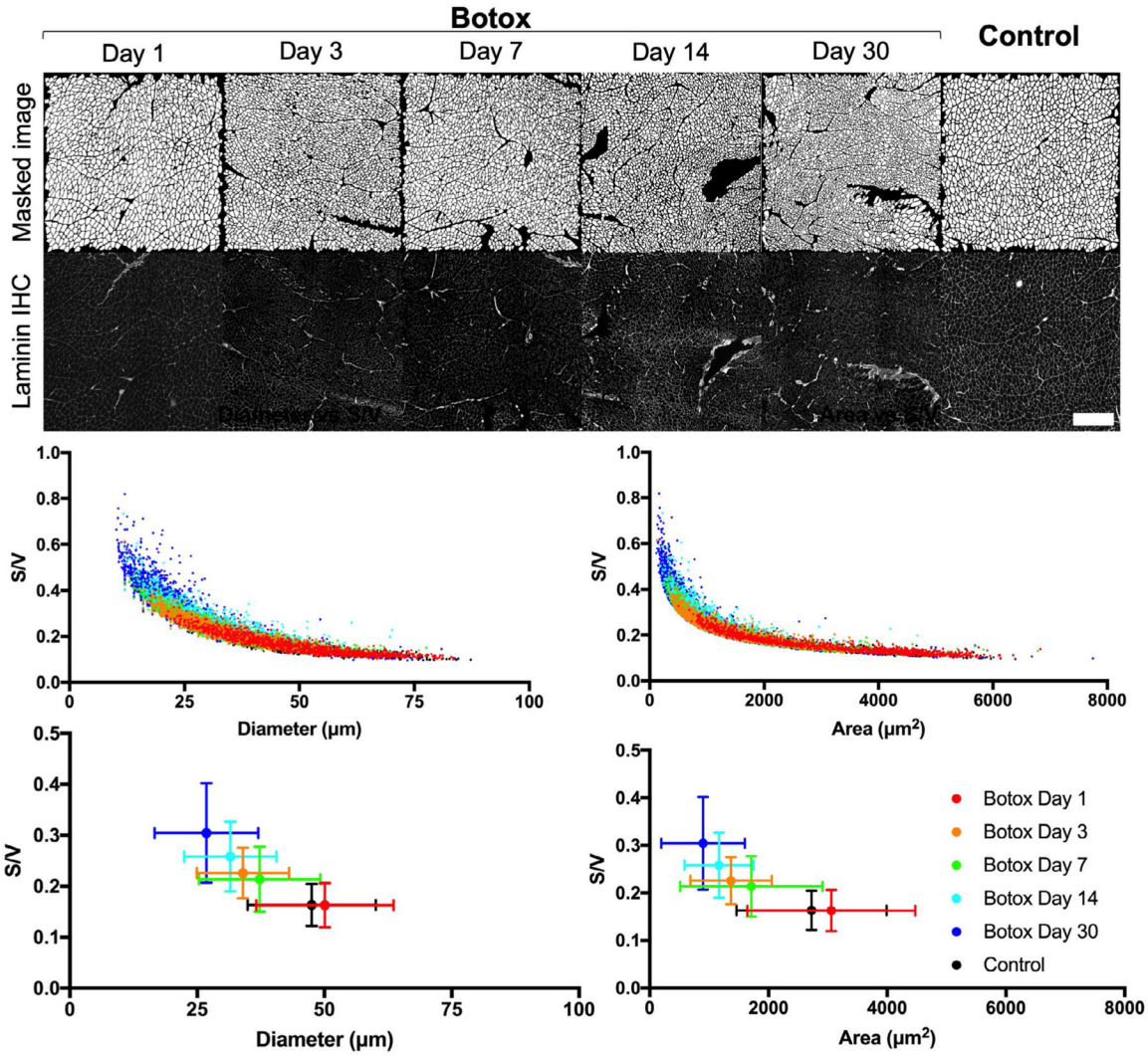

FIGURE 7.

Top) Supplemental analysis of 14,221 muscle fibers from immunohistochemistry of muscle fibers from botox injected and control skeletal muscle. Middle Left) Scatterplot depicting the surface area to volume ratio of all muscle fibers versus diameter. Nonlinear regression found $fiberdiameter = \frac{6.29}{S/V}$ with $R^2 = 0.895$. Middle Right) Scatterplot depicting the surface area to volume ratio of all muscle fibers versus fiber area. Nonlinear regression found $fiberarea = \frac{99.1m}{S/V}$ with $R^2 = 0.870$. Bottom Left) Averaged surface area to volume ratio and fiber size at each time point. Bottom RIght) Averaged surface area to volume ratio and fiber area at each time point. Scale bar = 500 μm

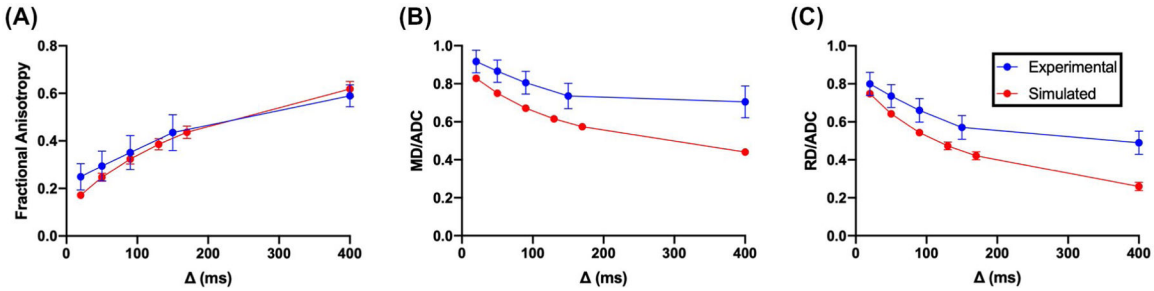

FIGURE 8.

Mean experimental and simulated results for FA (A), MD normalized by the ADC (B), and RD normalized by ADC (C). Overall, similar trajectories were observed for all parameters; however, experimental data had more variability at each diffusion time

TABLE 1

Extracellular water volume fractions applied to histology informed muscle models

	Day 1	Day 3	Day 7	Day 14	Day 30
Botox	**20**	15	10	10	10
Denervation	10	10	10	10	10
Tenotomy	10	5	5	5	5
Cardiotoxin	-	**45**	**35**	10	5

Extracellular water volume fractions were estimated from prior histology and MRI studies of these injury models at relevant time points. The volume fractions listed in bold are considered edematous (>20). The model with control geometry had 5% extracellular water volume fraction.

TABLE 2

Summary of DT measurements of general muscle injury models compared to control muscle

		DT (Δ)		
		Short	**Medium**	**Long**
		<90 ms	**130 ms-250 ms**	**>400 ms**
FA	Atrophy	+	+++	++
	Hypertrophy	−	−	−
	Edema	=/+	=/−	−
Diffusivity	Atrophy	−	−	−
	Hypertrophy	=/+	+	+
	Edema	=/−	=/+	+

+ Indicates that the diffusion measurement would increase relative to control muscle. − indicates that the diffusion measurements would decrease relative to the control muscle. The number of symbols is related to the approximate magnitude of the difference between control and injured muscles.